Nuclear Instruments and Methods in Physics Research A324 (1993) 482–490
North-Holland

NUCLEAR INSTRUMENTS & METHODS IN PHYSICS RESEARCH Section A

Optical properties of wavelength shifting panels

P. Soler and Z.H. Wang
School of Physics, University of Sydney, Sydney, NSW, 2006, Australia

Received 3 June 1992 and in revised form 21 August 1992

This paper describes the determination of the optical properties of the Bicron wavelength shifting acrylic plastic (BC-480) that absorbs ultraviolet radiation and then reemit it in the visible part of the spectrum. The refractive index and the attenuation coefficient as a function of wavelength were determined from transmission and reflection data. The reemitted visible spectrum was accurately measured using an optical multichannel analyzer and the quantum efficiency of the photoluminescence (the ratio between the number of emitted photons to the absorbed photons) was determined at different wavelengths in the ultraviolet. Finally, these results are applied to determine the effectiveness of this wavelength shifting panel as a means of detecting the ultraviolet component of the Cherenkov spectrum produced by a relativistic particle in water

1. Introduction

Wavelength shifters are often used in particle physics experiments to match the sensitivity spectrum of a detector to that of the emitted radiation. An important example of this type of application is the detection of Cherenkov radiation emitted by the passage of relativistic particles traversing a medium. Since more photons are emitted in the ultraviolet range than in the visible, and photomultiplier tubes are normally more sensitive in the visible (and near-UV), wavelength shifters can be used to reconcile this mismatch and hence increase the number of photoelectrons collected at the cathode.

The Falkiner High Energy Physics Department at the University of Sydney has constructed a prototype neutrino Cherenkov detector, SUNLAB, that uses pure water as a target for elastic scattering of neutrinos with electrons. As they recoil, the scattered electrons emit a Cherenkov signal that can be picked up by 54 photon collection units, consisting of an EMI 9623B photomultiplier tube (S11, 17.2 cm in diameter cathode) optically coupled to a 70 cm × 70 cm × 1.2 cm slab of Bicron BC-480 wavelength shifting panel. The details of this experiment can be found elsewhere [1].

It is very important to measure the optical properties of the wavelength shifting panels in order to fully understand the enhancement of the Cherenkov signal produced. In a previous paper [2], the bulk efficiency of converting Cherenkov photons into photoelectrons for the photon collection unit was measured to be 1.5% ± 0.5%, increasing the effective photomultiplier tube cathode area by, approximately, a factor of 3. It would be very valuable, however, to have a wavelength dependence of this response, as the Cherenkov spectrum is continuous and goes into the ultraviolet (see fig. 11). Also, the intrinsic optical properties of the BC-480 material are very important to know, because the amount of light collected inside the panel depends heavily on the refractive index and the attenuation coefficient.

For these reasons, in the present paper we will describe experiments to measure the refractive index and attenuation coefficients of the BC-480 wavelength shifting panels. In addition, the quantum efficiency from the photoluminescence of the panel (defined as the ratio between the number of emitted visible photons and the number of absorbed ultraviolet photons) was measured for different incident UV wavelengths. These wavelength dependent quantities are crucial in estimating the response of each of the photon collection units over all the spectral range of the Cherenkov light.

2. Refractive index and attenuation coefficient

Two samples of the Bicron BC-480 plastic, with thickness $h_1 = 2.396 \pm 0.004$ cm and $h_2 = 0.315 \pm 0.002$ cm, were cut and polished in order to carry out transmission and reflection measurements for the determination of their refractive index and attenuation coefficient. Because the thickness of these panels is much greater than the incident wavelength (200–800 nm) and these surfaces were not optically flat (due to slight undulations in the polished faces) the interference fringes produced by multiple reflections at both inter-

faces were not clearly visible. All the phase differences produced by all the partial waves inside the panel averaged out.

The total transmissivity T and reflectivity R, defined as the intensity of light transmitted or reflected with respect to the incident intensity across the whole panel, can be calculated as a function of the reflectivity ρ at each interface and the absorption coefficient α. By taking into account the addition of the intensity of all the partial waves transmitted and reflected [3], and knowing the thickness h of the sample, one can obtain the total transmissivity and reflectivity as:

$$T = \frac{(1-\rho)^2 \, e^{-\alpha h}}{1-\rho^2 \, e^{-2\alpha h}} \tag{1}$$

and

$$R = \frac{\rho\{1+(1-2\rho)\, e^{-2\alpha h}\}}{1-\rho^2 \, e^{-2\alpha h}}. \tag{2}$$

In general $R+T$ is less than one, so the amount of light absorbed inside the panel is given by:

$$A = 1 - R - T. \tag{3}$$

For perpendicularly incident light one can use one of the Fresnel formulae [4] to relate the reflectivity at the interface with the refractive index n of the panel inside an air medium:

$$\rho = \left(\frac{n-1}{n+1}\right)^2. \tag{4}$$

With eqs. (1), (2) and (4) we can deduce the absorption coefficient and refractive index of the panel from reflectivity and transmissivity data.

This data was acquired for the two samples mentioned before by using a Cary 2300 spectrophotometer manufactured by Variant Techtron Pty Ltd. The results of these measurements are plotted in fig. 1, where T_1 and R_1 refer to the thick 2.396 cm panel and T_2 and R_2 refer to the thinner 0.315 cm sample. The thickness of panels employed in the photon collection units is an intermediate one of 1.22 cm and hence will have transmissivity and reflectivity between the measured values.

From this figure one can see that there is a dramatic cutoff at around 400 nm below which the transparency of the panel becomes very small. The panel absorbs light below 400 nm very efficiently and then reemits it in the visible part of the spectrum where it is practically transparent, acting as a guide for the visible light.

The residual function

$$f(T_1, T_2) = (1/2)^{1/2}\left[\left(T_1 - \bar{T}_1\right)^2 + \left(T_2 - \bar{T}_2\right)^2\right]^{1/2},$$

where T_1, T_2 are the measured transmissivities and $\bar{T}_1$, $\bar{T}_2$ are the calculated ones from eq. (1), was minimized

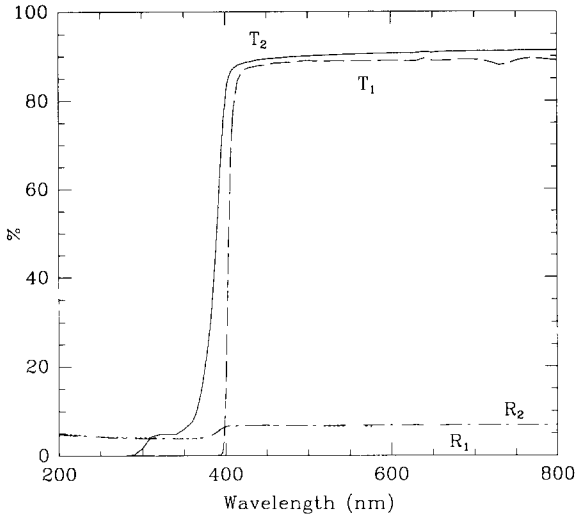

Fig. 1. Measured values of the transmissivity and reflectivity as a function of wavelength, for the thick 2.396 cm sample (T_1 and R_1) and for the thin 0.315 cm sample (T_2 and R_2) of Bicron BC-480 plastic.

to obtain an optimum value of the absorption coefficient for each wavelength. Using these values of the absorption coefficient, the residual function

$$f(R_1, R_2) = (1/2)^{1/2}\left[\left(R_1 - \bar{R}_1\right)^2 + \left(R_2 - \bar{R}_2\right)^2\right]^{1/2},$$

with R_1, R_2 the measured reflectivities and $\bar{R}_1$, $\bar{R}_2$ the calculated ones from eq. (2), was now minimized to optimize the reflectivity ρ at the interface and then eq. (4) was used to find the refractive index.

The values of the refractive index and absorption coefficient of the BC-480 plastic are plotted in figs. 2 and 3. A one oscillator model was fitted to the refractive index data. The expansion taken was found to agree with the following relation:

$$n^2 - 1 = A + \frac{B}{\lambda(\mathrm{nm})^2}, \tag{5}$$

with

$A = 1.0783 \pm 0.0008$

$B = 15810 \pm 140$,

and with $\chi^2 = 117$ for 55 degrees of freedom. The errors in the refractive index are larger than random errors because they represent the range of values consistent with the reflectivity measurements performed at the two different thicknesses (R_1 and R_2 in fig. 1). Points between 350 and 400 nm were found to have an unacceptably large uncertainty and were omitted (an estimate of the refractive index in this region may be done by utilising the fitted function of eq. (5)). Above 600 nm, because of the difference between R_1 and R_2, the errors in the refractive index were also found to be

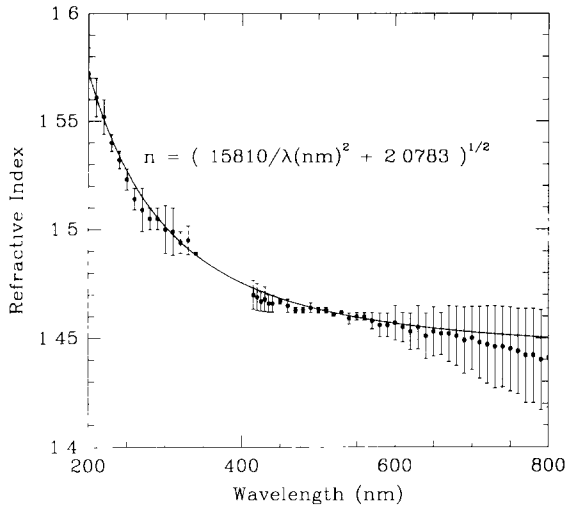

Fig. 2. Refractive index of the Bicron BC-480 plastic as a function of wavelength. A series expansion to a one oscillator model was fitted to the data points (solid line) and is also shown.

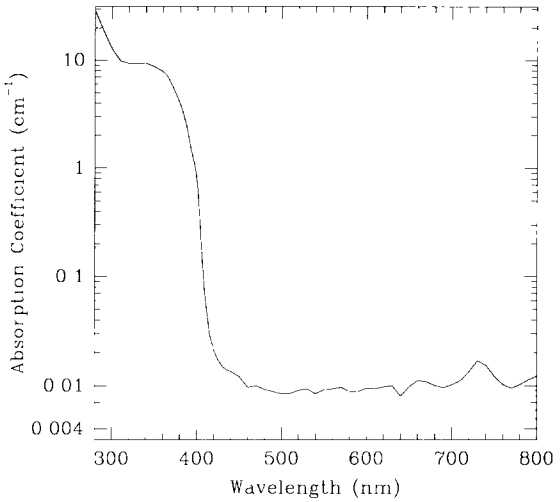

Fig. 3. Absorption coefficient of the Bicron BC-480 plastic as a function of wavelength.

large. However, between 400 and 500 nm, where the reemitted spectrum of visible light lies (see fig. 5), the refractive index measurements are well determined.

The refractive index at maximum emission (417 nm) is $n = 1.471 \pm 0.004$ while the absorption coefficient is 0.025 ± 0.004 cm^{-1}, which corresponds to an attenuation length between 33 and 46 cm. At even higher wavelengths the transparency is improved. Between 450 and 500 nm the attenuation length lies between 83 and 120 cm. It is also interesting to note that the absorption coefficient in the ultraviolet between 360 and 300 nm, lies between 7.8 and 12.8 cm^{-1}, which corresponds to an attenuation length between 1.3 mm and 0.8 mm. This means that in the near-UV region more than 90% of the light is absorbed within 2–3 mm.

The quoted value by the manufacturer for the refractive index is 1.49 (at an unspecified wavelength) [5], somewhat higher than our measured value in the visible. Also, a bulk attenuation length in the visible is given by the manufacturer to be 4.5 m. This value is also higher than the one deduced here. However, our values take into account the dispersion relations of the BC-480 for a wide range of wavelengths. It is worth noting, though, that taking the manufacturer's values into account and substituting these into eqs. (1) and (2) for the two samples we used, yields nearly identical results for the transmissivity (at 92%) and the reflectiv-

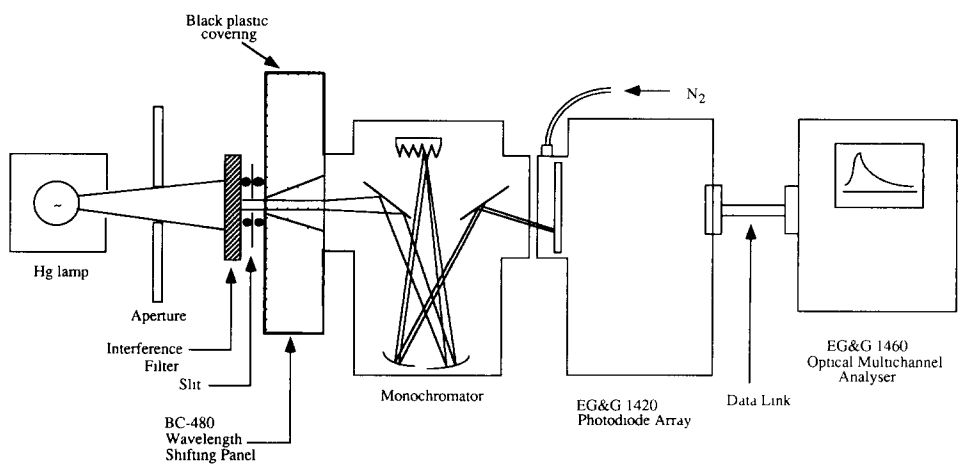

Fig. 4. Schematic diagram of the experimental arrangement used to measure the spectrum of the light reemitted by the Bicron BC-480 wavelength shifting panel.

ity (at 7.4%) for both samples. It is apparent from fig. 1 that we observe a clear difference between the two.

3. Emitted visible spectrum

To measure the spectrum of reemitted light from the BC-480 wavelength shifting panel the experimental arrangement shown in fig. 4 was used. A mercury lamp was used as the UV light source, with interference filters to select two different Hg lines at 365.0 ± 5.0 and 302.1 ± 5.0 nm (the second value quoted in both filters is half the full width at half maximum, FWHM, of the transmission). Also, 25 and 150 μm slits, respectively, were used to collimate the beam of UV photons perpendicularly to the wavelength shifting panel sample, which was in this case 1.216 ± 0.005 cm thick. Most of the UV photons are absorbed within the first 2 mm of entering the wavelength shifting panel and then reemitted isotropically in the visible. To ensure that no stray light entered the panel, black plastic completely covered the sample except for a small orifice where the entrance slit was attached and an exit hole for the emitted light. This was fastened in a light-tight manner to a monochromator coupled to an EG&G 1420, 1024 channel photodiode array connected to an EG&G 1460 optical multichannel analyzer. To keep the photodiode array free from moisture the EG&G 1420 unit was continuously purged with nitrogen gas.

The spectra were separated into two sections and were calibrated using three Hg lines, 365.05, 435.84 and 546.07 nm. The resolution in wavelength was then found to be 0.14 nm/channel. Combining both sections (from 365.0 to 435.8 nm and from 435.8 to 546.1 nm) and ensuring a smooth transition at 435.8 nm, a complete spectrum was obtained for both interference filters. As shown in fig. 8 the spectral response of the photodiode array (provided by the manufacturer) is not

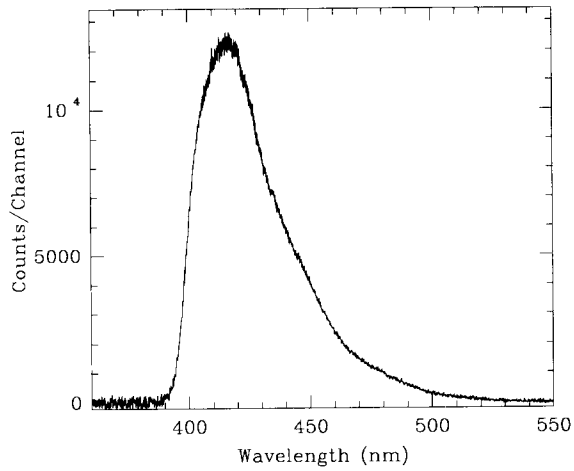

Fig. 5. Reemission spectrum of the Bicron BC-480 wavelength shifting panel after absorption of 302.0 nm UV radiation.

constant. Hence, the spectrum had to be corrected to take into account the sensitivity of the photodiode detectors. The corrected spectrum using 302.0 nm UV light as the source is plotted in fig. 5. Maximum emission occurs at 417 nm with half height wavelengths at 401 and 442 nm. The spectrum with the 365.0 nm interference filter was practically indistinguishable from the 302.0 nm spectrum and consequently would overlap with the one plotted in fig. 5. Thus we found that the emission spectrum is independent of the incident wavelength in the region between 300 and 365 nm.

This can be interpreted in the usual way for fluorescent materials by saying that the activator material deposited into the host plastic to convert it into a wavelength shifter introduces a set of intermediate energy levels between its valence and conduction band. If an electron is excited into the conduction band by the absorption of UV photons this can decay to the

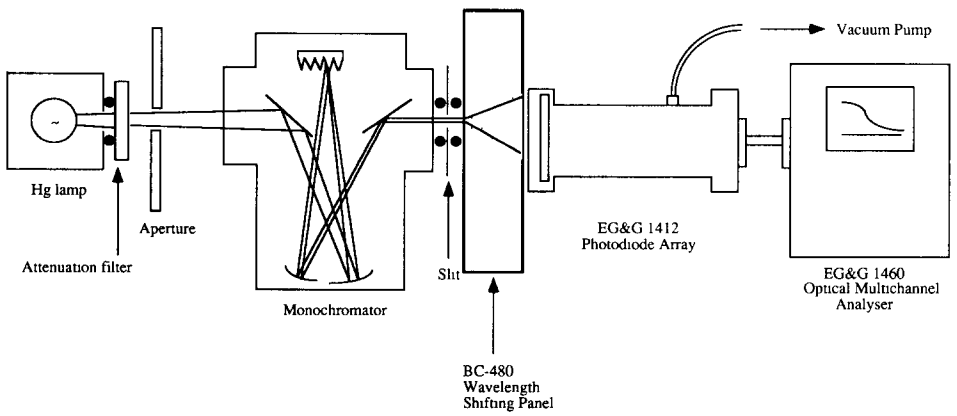

Fig. 6. Schematic diagram of the experimental arrangement used to measure the quantum efficiency of the photoluminescence from the Bicron BC-480 wavelength shifting plastic.

intermediate energy band and down to the valence band emitting a characteristic visible spectrum.

4. Quantum efficiency

The quantum efficiency of a photoluminescent material is defined as the ratio of the number of emitted photons to the absorbed photons assuming that all emitted photons escape, that is, none are absorbed in the phosphor [6].

The incident UV light sources were chosen from the UV lines of a mercury lamp. The 365.0, 302.1 and 253.7 nm lines were selected using bandpass interference filters with a FWHM of 10 nm, while lines at 334.1, 313.2 and 296.7 nm were singled out using a monochromator giving a resolution of 3 nm.

The aim of the experiment is to measure on the optical multichannel analyzer the intensity of the UV light going into the panel and to measure the intensity of the reemitted visible light in order to work out their ratio. Of course, due allowance has to be made for the different geometry and the different spectral responses in both cases. The experimental arrangement is shown in fig. 6. Note the difference between this set up and the one shown in fig. 4. The monochromator now acts as a UV light source and not as a detector of the emitted light. Also, an EG&G 1412 photodiode array attached to a vacuum pump (to ensure that the diodes remain free from moisture) was used as the light sensitive detector. For the measurements with the 365.0, 302.1 and 253.7 nm lines the monochromator was substituted by interference filters.

4.1. Measurements with the panel

When the panel is in place, the amount of light absorbed and the amount of light detected is affected by the following:

4.1.1. Initial interface

The transmission at the initial interface is going to be $96.0 \pm 0.1\%$ because the refractive index between 296 and 365 nm only varies from 1.50 to 1.49 (see fig. 2). The slits are all very small (25 to 500 μm), so the incidence can be assumed to be perpendicular, and eq. (4) can be used reliably to calculate the transmission.

4.1.2. Light escaping panel

The light that escapes the panel has to be emitted within a 43° angle with respect to the perpendicular ($n = 1.471$ at visible wavelengths). Any light trying to exit the panel with greater angles is trapped within by total internal reflection. Of the light that does escape, however, only a fraction is seen by the photodiode array, depending on the distance D of the panel to the detector. The light is refracted outwards at the interface so the detector only sees light that was initially emitted within a cone with a critical half-angle θ_c (see fig. 7). For a typical distance of about 12 mm, this critical angle is around 30°.

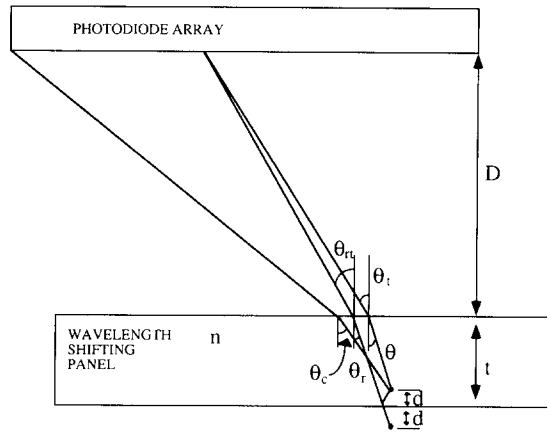

Fig. 7 Geometry involved in the detection by the photodiodes of the emission of light from the wavelength shifting panel.

Since the light that escapes the panel is no longer perpendicular, Fresnel's laws have to be taken into account [4]. Assuming no polarization (the light is emitted isotropically) the expression for the transmissivity at the interface is then:

$$\tau(\theta) = \frac{2n \cos\theta_t \cos\theta}{[\cos\theta + n\cos\theta_t]^2} + \frac{2n \cos\theta_t \cos\theta}{[n\cos\theta + \cos\theta_t]^2}, \tag{6}$$

where n is the panel's refractive index, θ is the angle of incidence and θ_t is the transmitted angle given by Snell's law:

$$\sin\theta_t = n \sin\theta. \tag{7}$$

The illuminance E_F collected by the detector due to light being transmitted in this forward cone is then:

$$E_F(\theta) = I\tau(\theta)\, d\Omega/dS, \tag{8}$$

where I is the emitted intensity, $d\Omega$ is the unit solid angle of emission and dS is the unit area of collection on the detector. If D is the distance from the panel to the detector, t is the thickness of the panel and d is the distance travelled by the light in the panel before being absorbed, the geometry is given by fig. 7 and the illuminance collected turns out to be:

$$E_F(\theta) = \frac{I\tau(\theta)\cos^4\theta_t}{Dn[(t-d)\cos\theta_t + Dn\cos\theta]}. \tag{9}$$

There is also a certain amount of light collected at the detector due to reflections off the back wall of the panel. This is identical to the emission produced by a virtual absorption centre a distance d behind the back

interface, where due allowance is made for the reflectivity $\rho(\theta) = 1 - \tau(\theta)$ at that interface (see also fig. 7). The angle θ_r needed for a reflected ray to reach the detector at the same place as a ray in the forward direction with angle θ is given by:

$$\theta_r = \theta - \frac{d \sin 2\theta}{(t-d) + Dn(\cos^3\theta)/(\cos^3\theta_t)}. \quad (10)$$

The angle θ_r is slightly smaller (about 1° less) because the emitting centre seems to be further away. The illuminance collected at the detector due to the light being reflected from the backward cone is calculated the same way as with eq. (9), and yields:

$$E_B(\theta_r) = \frac{I\tau(\theta_r)\rho(\theta_r)\cos^4(\theta_{rt})}{Dn[(t+d)\cos\theta_{rt} + Dn\cos\theta_r]}, \quad (11)$$

where θ_r is given in eq. (10) and θ_{rt} is given by Snell's law:

$$\sin\theta_{rt} = n \sin\theta_r. \quad (12)$$

The total light collected at the detector will then be the contribution of both the forward and backward cone:

$$E(\theta) = E_F(\theta) + E_B(\theta_r). \quad (13)$$

where $E_F(\theta)$ is given in eq. (9) and $E_B(\theta_r)$ comes from eq. (11).

The fraction of light that the photodiode array observes is given by the ratio of solid angles. A quantity, collection efficiency ϵ_{coll} of the detector, can be defined as:

$$\epsilon_{coll} = \frac{\int_F \tau(\theta)\,d\Omega + \int_B \tau(\theta_r)\rho(\theta_r)\,d\Omega_r}{\int_{TOTAL} d\Omega}, \quad (14)$$

where F refers to integrating the forward cone yield and B refers to the backward cone. This quantity takes into account the geometry of the experimental arrangement and is a measure of the percentage of the emitted light that is collected at the detector. This value was different for every case and depended on the alignment of the beams and the distance to the detector (which varied minimally). Typically this collection efficiency varied between 6% and 9%, with 96% of the light detected coming from the forward cone and 4% of the light coming from the backward cone. Any multiple reflections have been neglected.

4.1.3. Sensitivity of the detector to the emitted spectrum

Since we want to compare the output of light in the visible to the incident UV light, it is necessary to know the sensitivity of the detector as a function of wavelength. This is provided by the manufacturer and can be seen in fig. 8. From this data we can obtain the average sensitivity due to the emitted spectrum shown in fig. 5. This value was found to be 4.75×10^{-4} counts/photon.

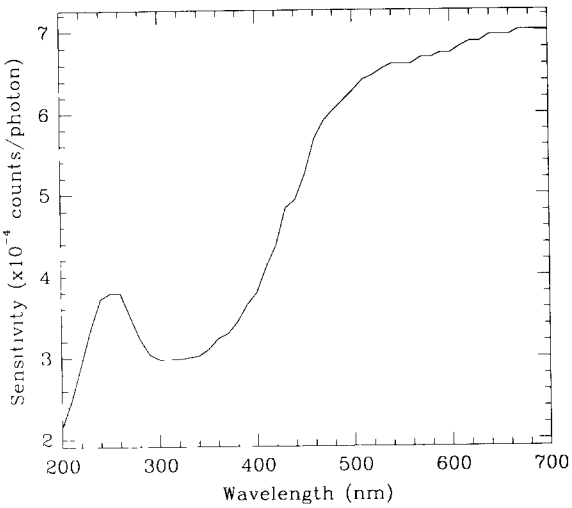

Fig. 8. Sensitivity of the 1024 channel EG&G 1420 photodiode array, as provided by the manufacturer.

4.2. Measurements without the panel

To compare the total number of photons emitted by the panel with the number of photons that impinge upon it we have to measure this under the same conditions as before but removing the wavelength shifting panel from the arrangement. While taking measurements of the incident UV light under these conditions (at 365.0, 334.1, 313.2, 302.1, 296.7 and 253.7 nm) we had to take into account additional factors:

4.2.1. Attenuating filters

To ensure that the response of the photodiodes did not saturate, additional attenuating filters (Wratten type 18A and 3) were introduced. The characteristics of these were measured with the Cary 2300 spectrophotometer and the average attenuation at each particular wavelength was calculated.

4.2.2. Sensitivity of the detectors in the UV

By folding in the very narrow spectral profile of the incident UV beam across its bandwidth with the given sensitivity of the detector (fig. 8), one can obtain average sensitivities for each of the UV lines being used. The values lie between 3.0×10^{-4} counts/photon and 3.3×10^{-4} counts/photon. One can see that the photodiodes are 1.5 times more sensitive in the visible part of the spectrum than in the UV.

4.3. Results

The emitted visible light was collected by the photodiode array using the geometry shown in fig. 7. The

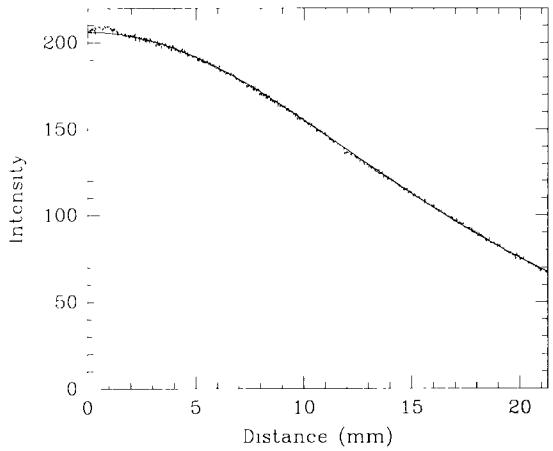

Fig. 9. Typically measured response of the photodiode array to the reemitted light from a slab of Bicron BC-480 wavelength shifting panel (dotted line). The intensity of the response of each photodiode is plotted against the distance between the diode and the centre of the beam used to align the array. Superimposed (solid line) is the expected response derived by taking into account Fresnel's laws at the interfaces and the illuminance collected by the detector.

detector was aligned so that a beam of light going through the panel would be registered on one side of the 1024 channel photodiode array. Since the array is 1 in. long this gives an effective spatial resolution of 25 μm. As a consequence of this arrangement, when UV light was being reemitted by the panel the detector only saw half the emitted cone.

The response of the photodiode array to the reemitted light is seen in fig. 9. Superimposed on it is the expected response derived from eqs. (9)–(13). Each time the beam was aligned, the distance from the panel to the detector was changed slightly, and the expected response was optimized to the observed one, that way obtaining the best value for the distance. The response curve was then integrated to achieve the total recorded intensity, and by taking into account the collection efficiency (for the optimized distance) a total emitted yield was deduced for each case.

As can be seen from fig. 9 the observed and expected response curves agreed very well. This ensured that the geometry of the detection system was well understood and hence the panel quantum efficiencies derived were deemed to be reliable. The total UV yield was also measured. This was just a beam of UV light with a fairly flat response and whose half width was typically 2.5 mm. This was also integrated to obtain the total UV yield for each wavelength. The ratio between the total emitted yield and UV yield gives the efficiency after taking into account the sensitivity of the detector, the initial interface and any attenuating filters used.

Table 1
Summary of all the quantum conversion efficiencies corresponding to UV light of different wavelengths

Wavelength [nm]	Quantum conversion efficiency [%]
365.0 ± 5.0	43.1 ± 2.6
334.1 ± 1.5	20.0 ± 1.1
313 2 ± 1.5	16.8 ± 1 0
302.1 ± 5.0	9.8 ± 2.2
296.7 ± 1.5	8.9 ± 1.4
253.7 ± 5.0	1.5 ± 0.8

Runs were performed for the six UV wavelengths using both sides of the photodiode array (to compensate for any bias produced by different responses of the individual photodiodes). A weighted average of these runs was performed and the results are shown in table 1 and plotted in fig. 10. Superimposed one can see a quadratic fit to the data. This functional relation is useful as an empirical model of the quantum conversion efficiency of the wavelength shifting panel. If the wavelength is expressed in nm the efficiency expressed as a percentage becomes:

$$\epsilon(\lambda) = C_0 + C_1\lambda + C_2\lambda^2\% \quad (248\ \text{nm} < \lambda < 400\ \text{nm})$$

where

$$C_0 = 163 \pm 47, \qquad (15)$$
$$C_1 = -1.34 \pm 0.30, \text{ and}$$
$$C_2 = (2.76 \pm 0.49) \times 10^{-3},$$

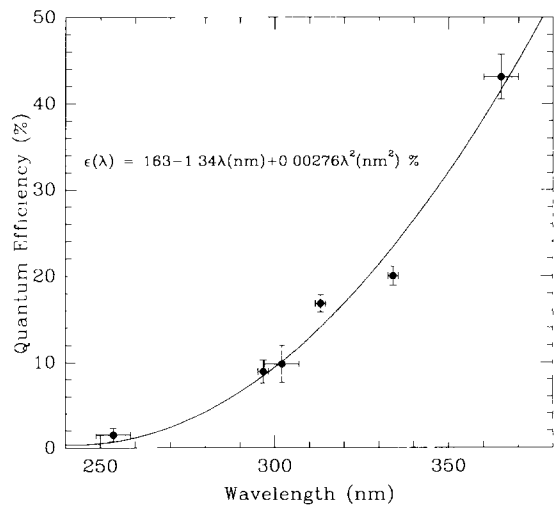

Fig. 10. Measured quantum conversion efficiency of the photoluminescence from the Bicron BC-480 wavelength shifting panel as a function of incident wavelength An empirical fit was performed to this data and is shown as a solid line on the graph.

and with $\chi^2 = 8.0$ for 3 degrees of freedom. One can see that the efficiency diminishes as the wavelength diminishes, implying that the probability of non-radiative decays increases for absorbed photons of higher frequencies.

5. Discussion

As mentioned before, these wavelength shifting panels are coupled to photomultiplier tubes to record the signals from a water Cherenkov detector. The spectrum of the Cherenkov signals is therefore distorted due to the non-constant response of the wavelength shifting panel. The number of Cherenkov photons emitted by electrons in water [7] is given by:

$$N = 2\pi\alpha L \int_{\lambda 1}^{\lambda 2} \left[1 - \frac{1}{n(\lambda)^2 \beta^2}\right] \frac{d\lambda}{\lambda^2}, \qquad (16)$$

where λ is the wavelength of the emitted photon, $\alpha = 1/137$, the fine structure constant, $n(\lambda)$ is the refractive index of water, β the velocity of the electron with respect to the speed of light and L is the length of the electron's track in the water.

From the observed efficiencies one can obtain a BC-480 wavelength shifting panel modified Cherenkov spectrum for the UV range. This is shown in fig. 11, where we have assumed all electrons are ultrarelativistic ($\beta = 1$). Instead of having the typical $1/\lambda^2$ dependence, below the UV absorption wavelength of 400 nm the response gradually decreases with diminishing wavelength up to the cutoff around 250 nm.

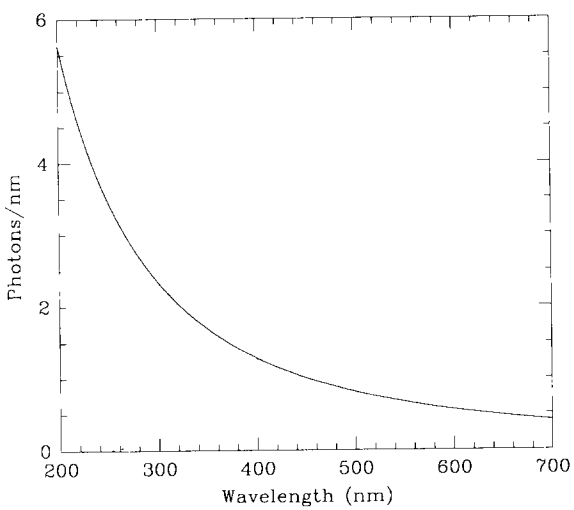

Fig. 11. Spectrum of the emission of Cherenkov radiation by a relativistic particle travelling in 1 cm of water (solid line). The effect of the Bicron BC-480 wavelength shifting panel below 400 nm, where the absorption and reemission of the radiation becomes important, is also shown (dotted line).

This means that out of a possible 535 Cherenkov photons between 200 and 400 nm emitted by an electron travelling in one cm of water (216 are emitted between 400 and 700 nm), only 60 can be detected by the panel. The photon collection units used in the water Cherenkov detector are 70 cm × 70 cm panels coupled to a photomultiplier tube with a 17.2 cm cathode diameter [1]. The radial response of these photon collection units when submerged in water was measured in ref. [2]. It was found that if a flash of light impinges upon the edge of the panel and the light is piped through multiple reflections to the cathode the response is 33% of the same event occurring directly in front of the cathode. Using these parameters one can estimate that the effective photocathode area is increased by a factor of 3.1 by utilizing the wavelength shifting panel. This is in agreement with the previous estimate between 3 and 4 found in ref. [2]. One has to note though, that this is an upper limit because there is a further degradation of the UV light inside the water and this depends on the distance between the emitted light and the photon collection unit.

The Cherenkov detector was carefully modelled in ref. [1] with Monte Carlo techniques. The expected response of the panel was used in the simulation and it was found that the effective detection threshold for recoil electrons could be lowered to 6.0 MeV. This is a direct consequence of using the wavelength shifting panels and is crucial in determining the feasibility of building a modular Cherenkov detector sensitive to solar neutrinos.

6. Conclusion

The optical properties of the Bicron BC-480 wavelength shifting panels have been determined. From reflection and transmission measurements we have been able to determine the refractive index and absorption coefficient in the ultraviolet and visible part of the spectrum. The refractive index between 400 and 500 nm remains fairly constant at 1.471 ± 0.004. The attenuation length in this same part of the spectrum lay between 40 and 120 cm.

The Bicron BC-480 absorbs UV light and reemits it isotropically in the visible. The emitted photoluminescent spectrum was measured and it was found to be independent of the incident UV wavelength. Maximum emission was found at 417 nm with half height wavelengths at 401 and 442 nm.

The quantum efficiency of the emission, defined as the ratio of emitted photons to absorbed photons, was also determined for different wavelengths. This efficiency was found to vary, from a value of 43% at 365

nm down to 1.5% at 254 nm. The consequence is that if this wavelength shifting panel is used to detect the Cherenkov emission of electrons in water, the Cherenkov spectrum is distorted by the varying efficiency. Despite this distortion, the inclusion of the BC-480 panels for our Cherenkov detector increases the photocathode coverage by a factor of 3.1. This factor is crucial in lowering the effective energy threshold of recoil electrons that can be detected by the water Cherenkov detector down to 6 MeV.

Acknowledgements

We wish to thank Dr. S. White for helping in the transmissivity and reflectivity measurements and Associate Professor L.S. Peak for many helpful discussions. The authors acknowledge financial support from the Australian Postgraduate Research Awards Scheme and from His Royal Highness Prince Nawaf Bin Abdul Aziz of the Kingdom of Saudi Arabia through the Science Foundation for Physics within the University of Sydney.

References

[1] A.M. Bakich, R.C. Cederblad, P.R. Gerhardy, J. Malos, M. Omori, L.S. Peak, C.J Sheerman and P. Soler, Nucl Instr. and Meth. A273 (1988) 853.
[2] A.M. Bakich and L.S. Peak, Nucl. Instr. and Meth. A247 (1986) 334.
[3] L Levi, Applied Optics (A Guide to Optical System Design), vol. 2 (Wiley, 1980).
[4] M. Born and E. Wolf, Principles of Optics, 6th ed. (Pergamon, 1980).
[5] Bicron Corporation Product Catalogue (1990).
[6] L. Levi, Op. Cit., vol. I
[7] J.V. Jelley, Cherenkov Radiation and its Applications (Pergamon, 1958).